Biophysical Journal Volume 83 August 2002 1184–1193

Probing the Endocytic Pathway in Live Cells Using Dual-Color Fluorescence Cross-Correlation Analysis

Kirsten Bacia,* Irina V. Majoul,† and Petra Schwille*
*Experimental Biophysics Group, †Department of Neurobiology, Max-Planck-Institut für biophysikalische Chemie, D-37077 Göttingen, Germany

ABSTRACT Fluorescence (auto)correlation spectroscopy (FCS) has developed into a widely used method for investigating molecular dynamics and mobility of molecules in vitro and in vivo. Dual-color cross-correlation, an extension of this technique, also assesses the concomitant movement of two spectrally distinguishable fluorescent molecules and has therefore proven superior to autocorrelation analysis to study interactions between different molecular species in solution. Here we explore the benefits of cross-correlation analysis when applied to live cells, by demonstrating its potential in analyzing endocytic processes. Bacterial cholera toxin (CTX) was labeled with Cy2 and Cy5 dyes on different subunits of the same holotoxin. Along the endocytic pathway, positive cross-correlation between the A and B subunits was first preserved, later followed by a loss in cross-correlation upon their separation in the Golgi. Furthermore, endocytosis of a mixture of only Cy2- and only Cy5-labeled holotoxins also gave rise to cross-correlation. Our results suggest that cross-correlation may be used to recognize whether different cargoes use the same endocytic pathway. Additionally, we show that cross-correlation is applicable to two-dimensional membrane diffusion. CTX bound to GM1-containing artificial giant unilamellar vesicles was diffusible, whereas CTX bound to the plasma membrane was immobile on the FCS time-scale, possibly because of raft-association of GM1.

INTRODUCTION

Fluorescence correlation spectroscopy (FCS, Magde et al., 1972) assesses molecular mobility and dynamics of fluorescently labeled biomolecules at low concentrations (Elson and Magde, 1974; Eigen and Rigler, 1994; Schwille, 2001a). As an optical technique with minimal disturbance of the system, FCS offers a great potential for studying biomolecules in their natural environment in living cells. Previously, a number of in vivo applications have been demonstrated (Brock et al., 1998; Widengren and Rigler, 1998; Schwille et al., 1999a,b; Wachsmuth et al., 2000), despite experimental difficulties induced by the intracellular environment. These include cellular autofluorescence, increased photobleaching attributable to slowed diffusion, and dye depletion attributable to limited cellular volumes (Schwille et al., 1999a; Schwille, 2001a). However, it is often difficult to assign the observation of variations in molecular mobility to clearly defined processes in the complex intracellular environment. Differences in molecular mobility may be attributed to interactions of the probes with organelles, with known or yet unidentified molecules, or may be attributable to local confinement to small compartments. For instance, obstruction of intracellular diffusion has been found for eGFP and eGFP-fusion proteins, especially in the nucleus (Wachsmuth et al., 2000) and for a fluorescent lipid analogue diffusing in the plasma membrane (Schwille et al., 1999b).

Dual-color cross-correlation spectroscopy (Schwille et al., 1997; Schwille, 2001b; Kettling et al., 1998; Heinze et al., 2000) is a conceptual extension of standard FCS using two instead of one fluorescent species. Whereas in autocorrelation analysis, the fluorescence signal fluctuating in time is compared with *itself*, in dual-color cross-correlation the fluorescence signals originating from two spectrally distinguishable labels are compared with one another. Cross-correlation analysis reports the concomitancy of the movement of the two species under investigation on the spatial scale of the detection volume, in addition to their mobilities and internal dynamics. Despite the known difficulties of applying standard FCS to in vivo systems (Schwille et al., 1999a), the in vivo application of dual-color cross-correlation analysis is expected to allow for a much more detailed and reliable study of intracellular interactions. Here we show for the first time the intracellular use of dual-color cross-correlation spectroscopy as applied to the phenomenon of toxin endocytosis, and we discuss important experimental and theoretical issues in this context.

Traditionally, different fluorescence spectroscopic techniques have been used to detect the association of proteins or protein subunits. Using fluorescence resonance energy transfer (FRET), Bastiaens et al. (1996) previously showed that the A and B subunits of cholera toxin (CTX) remain associated from the plasma membrane to the Golgi apparatus and subsequently become separated. However, in this study, endocytosis could not be followed in vivo in real time, because the cells had to be fixed after variable incubation times, and the acceptor irreversibly bleached to record an increase in donor fluorescence. Furthermore, FRET is limited to maximum

Submitted January 17, 2002 and accepted for publication March 27, 2002.
Address reprint requests to Petra Schwille, Max-Planck-Institut für biophysikalische Chemie, Am Fassberg 11, D-37077 Göttingen, Germany. Tel.: 49-551-201-1165; Fax: 49-551-201-1435; E-mail: pschwil@gwdg.de.

0006-3495/02/08/1184/10 $2.00

distances between the chromophores of several nanometers and is therefore critically dependent on protein dimensions and labeling. In contrast, cross-correlation analysis can detect the codiffusion of differently labeled molecules in the same small vesicle and of molecules bound to one another. In this respect, cross-correlation is less distance-specific and thus more versatile than FRET as a technique.

CTX belongs to the family of bacterial toxins that exhibit an AB-structure. These toxins have become popular for studying vesicular transport pathways and cytosolic delivery (Schiavo et al., 2001). The B portion or subunit of these types of toxins is required for membrane binding and cellular uptake of the toxin, whereas the A subunit carries out the enzymatic reaction once it has reached the cytosol. Different toxins offer unique opportunities for studying intracellular transport, because they exploit different pathways in the host cell to reach their sites of action. CTX is believed to use a retrograde pathway via endosomes and the Golgi to the endoplasmic reticulum (Majoul et al., 1996; Lencer et al., 1999).

CTX is formed by an isopentameric B_5 subunit with a molecular mass of 5×11 kDa and a 28.5-kDa A subunit. The A subunit consists of two peptides linked by a disulfide bond, from which the enzymatically active A1 peptide (Fontana et al., 1995) is liberated by reductive cleavage. For our experiments, we used the S63K mutant that lacks the ADP-ribosylation activity of the A1-peptide to avoid cAMP effects on intracellular transport. The B_5 subunit is responsible for cell surface-binding through interaction with GM1 ganglioside molecules.

Two different cases were studied by dual-color cross-correlation spectroscopy. In the first case, A and B subunits of the holotoxin were labeled with the spectrally well separated indocarbocyanine dyes Cy2 and Cy5, respectively. The double-labeled toxin CTA-Cy2–CTB-Cy5 was added to live Vero cells. Unbound excess of the toxin was washed away, and endocytosis was followed using laser scanning microscopy (LSM). Fluorescence cross-correlation measurements were performed at successive time points and at different positions in the same cell to determine at what stage in the endocytic pathway the A and B subunits of CTX diverge. Only as long as the A and B subunits comigrate, either bound to one another or confined to the same diffusing compartment, can positive cross-correlation be observed. In the second case, the endocytosis of two differently labeled cargoes, cholera holotoxin labeled only with Cy2 and cholera holotoxin labeled only with Cy5, was studied. Because CTX-Cy2 and CTX-Cy5 differ only with respect to their labels, they take the same endocytic route and become localized in the same small diffusing vesicles and therefore show intracellular cross-correlation.

MATERIALS AND METHODS

Cell culture

Vero cells (African green monkey kidney cells; ECACC 84113001) were grown in DMEM (GibcoBRL, Life Technologies, Rockville, MD) with 2 mM glutamine, 10% fetal calf serum, 100 U/ml penicillin, 0.1 mg/ml streptomycin at 10% CO_2 and 37°C. Cells were transferred to phenol-red free medium and plated on round 25-mm coverslips. Cells were mounted in custom-made chambers for imaging and FCS measurements.

CTX labeling and purification

CTX mutant S63K (Fontana et al., 1995; kindly provided by M. G. Pizza) lacking ADP-ribosylation activity was used to avoid cAMP effects on intracellular transport.

The toxin was equilibrated with 0.1 M bicine buffer, pH 8.5, and incubated shortly with a fivefold excess of Cy5 monosuccinimidyl ester (Amersham Pharmacia Biotech, Piscataway, NJ) to label specifically the B subunit. Excess dye was washed away and the sample was rebuffered to pH 7.8 using Centricon 30 (Millipore, Bedford, MA). To protect the prelabeled subunit, the sample was incubated with Fab fragments of antibodies against the B subunit. The mixture was then reacted with a 10-fold excess of Cy2 for 30 min to specifically label the A-subunit. Double-labeled CTX was purified from unbound Cy2 by gel filtration. Fab fragments were dissociated from the toxin by incubation in 0.1 M citrate, pH 3.5, and the double-labeled CTX was rapidly purified from unbound Fab fragments and dissociated CTX subunits by centrifugal filtration through Centricon 50. Single-labeled cholera holotoxin was prepared in a similar manner, but without antibody protection.

Characterization of double-labeled CTX

To test for the specificity of A and B subunit labeling, double-labeled CTX was separated by 15%-polyacrylamide gel electrophoresis in the presence of reducing agents. Fluorescence from the gel bands was analyzed using the LAS-1000 charge-coupled device system (Fuji, Tokyo, Japan), equipped with a mercury lamp and corresponding Cy2 and Cy5 optical filter sets. Up to 85% of specific labeling of A and B subunits was detected with no labeling of the A2 fragment (5.5 kDa).

CTX that had been double-labeled in this manner showed cross-correlation. Temperature denaturation caused the cross-correlation amplitude to subside (data not shown). Measured diffusion times indicated that this was attributable to subunit-separation rather than fluorescent labels being released from the proteins.

Giant unilamellar vesicles (GUVs)

GUVs were prepared from DLPC (1, 2-dilauroyl-*sn*-glyero-3-phosphocholine, Avanti Polar Lipids, Alabaster, AL) and 0.01 mol% ganglioside GM1 (Calbiochem, San Diego, CA), with the addition of 5 mol% DPPS (1, 2-dipalmitoyl-*sn*-glycero-3-phosphoserine, from Avanti Polar Lipids) essentially according to Akashi et al. (1996). A charged lipid like DPPS is necessary for obtaining GUVs by this method. Briefly, lipids were dissolved at 10 mg/ml in chloroform:methanol (2:1). 100 μl of this solution was dried overnight in a rotary evaporator at 45°C to form a thin lipid film. The dried film was hydrated with preheated buffer (50 mM KCl, 5 mM PIPES, pH 7.0) and kept at 37°C for several hours. Some of the cloudy solution containing the giant liposomes was harvested and transferred to Lab-Tek coverglass chambers (Nalge Nunc, Naperville, IL) for measurements. Vesicles for control experiments were prepared without GM1.

Vesicles and cells were checked for autofluorescence in the laser scanning microscope before the addition of labeled CTX. CTX in phosphate-buffered saline was added and (in the case of the cells) washed away

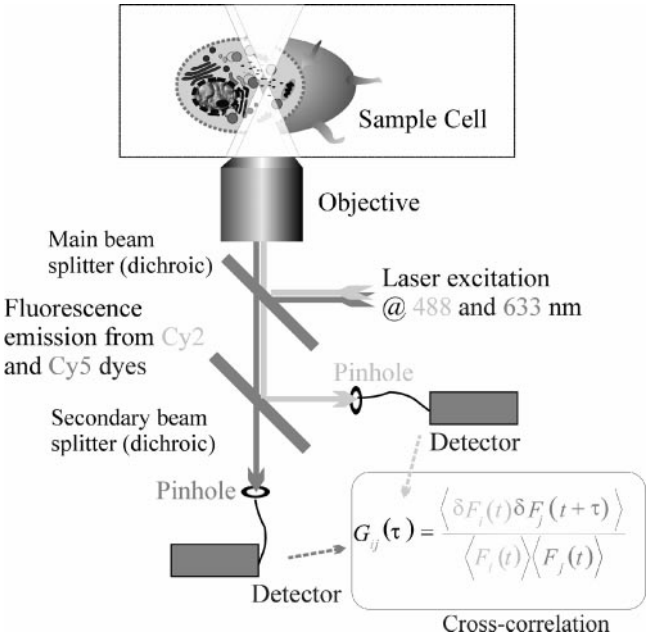

FIGURE 1 Setup. Schematic representation of the ConfoCor2 setup used for dual-color cross-correlation analysis.

with phosphate-buffered saline after a few minutes of incubation. Binding was specific, as assessed by LSM. CTX was bound to the cell plasma membrane and to vesicles containing GM1, but not to vesicles prepared without GM1.

Experimental setup for FCS

LSM and FCS were performed on a commercial ConfoCor2 combination system (Zeiss, Jena, Germany), using the cross-correlation configuration (Fig. 1). The 488 nm line of an Ar-Ion Laser and a 633 nm HeNe Laser were attenuated by an acousto-optical tunable filter to ~13 and 2 μW, respectively, reflected by a dichroic mirror (main beam splitter 488/633) and focused through a Zeiss C-Apochromat 40×, NA 1.2 water immersion objective onto the sample. The fluorescence emission was split by a second dichroic mirror (secondary beam splitter 635), passed through a 505–550-nm bandpass and a 650-nm longpass filter, respectively, and recorded in two separate channels. Out-of plane fluorescence was considerably reduced by two pinholes, each set at 90 μm in diameter. Detection was achieved using two avalanche photodiodes. The signals were software-correlated, and the individual autocorrelations as well as the cross-correlation curve were displayed online. The $1/e^2$ lateral radii of the detection volumes were determined to be ~0.18 μm (488-nm excitation) and 0.25 μm (633-nm excitation) from calibration measurements using standard dyes (Alexa 488, Molecular Probes, Eugene, OR; Cy5, Amersham Pharmacia Biotech). For intracellular measurements, the desired measurement position was chosen in the LSM image, using the automated stage positioning feature of the ConfoCor2 system. For membrane measurements, the FCS focus was positioned using an axial (z-) scan through the membrane as described in Schwille et al. (1999b). Data were evaluated by Levenberg-Marquardt nonlinear least-squares fitting to the appropriate model equations, using the ConfoCor2 or Origin software (OriginLab, Northampton, MA).

Theoretical concept of fluorescence auto- and cross-correlation spectroscopy

The principles of FCS in confocal setups have been previously described in a number of articles and reviews (Elson and Magde, 1974; Thompson, 1991; Rigler et al., 1993; Elson and Rigler, 2001). FCS analyzes spontaneous temporal fluctuations in the fluorescence emission signals $F_i(t)$ from small ensembles using the general correlation function:

$$G_{ij}^{F}(\tau) = \langle F_i(t)\cdot F_j(t+\tau)\rangle/(\langle F_i\rangle\cdot\langle F_j\rangle)$$

or

$$G_{ij}^{\delta F}(\tau) = \langle \delta F_i(t)\cdot \delta F_j(t+\tau)\rangle/(\langle F_i\rangle\cdot\langle F_j\rangle) = G_{ij}^{F} - 1 \quad (1)$$

where $\langle\ \rangle$ denotes the time average, $\delta F(t) = F(t) - \langle F(t)\rangle$ the fluctuations of $F(t)$, $i = j$ in the case of autocorrelation, and $F(t)$ is assumed to be constant over long-time averages.

In the case of fluctuations arising from free Brownian diffusion of i different species of fluorescent molecules with fractions Y_i and brightness parameters η_i through the detection volume, the model equation for fitting the experimental autocorrelation curves obtained in commonly used confocal setups reads (Schwille et al., 1997):

$$G_{\mathrm{Diff}}(\tau) = \frac{1}{N_{\mathrm{total}}}\left(\sum_i Y_i\eta_i^2\mathrm{Diff}_i(\tau)\right)\Big/\left(\sum_i Y_i\eta_i\right)^2 \quad (2)$$

with

$$\mathrm{Diff}_i(\tau) = \left(1+\frac{\tau}{\tau_{\mathrm{diff,i}}}\right)^{-1}\cdot\left(1+\frac{\tau}{SP^2\cdot\tau_{\mathrm{diff,i}}}\right)^{-1/2} \quad (3)$$

for three-dimensional (3-D) diffusion, with the structure parameter $SP = z_o/\omega_o$, where z_o and ω_o are the axial and lateral $1/e^2$ parameters of the Gaussian detection volume, respectively.

In the limit of a large structure parameter SP or 2-D diffusion as found in membranes, Eq. 3 reduces to

$$\mathrm{Diff}_i = \left(1+\frac{\tau}{\tau_{\mathrm{diff,i}}}\right)^{-1} \quad (4)$$

In many cases, intramolecular dynamic processes involving dark states, such as triplet states (Widengren et al., 1995) or conformational isomers (Schwille et al., 2000; Widengren and Schwille, 2000), require the incorporation of one or more exponential decay terms to the correlation function:

$$G_{\mathrm{Diff,blinking}}(\tau) = \frac{1-F+F\cdot e^{-\tau/\tau_b}}{1-F}\cdot G_{\mathrm{Diff}}(\tau) \quad (5)$$

From the diffusion time of a species, $\tau_{\mathrm{diff,i}}$, the diffusion coefficient can be calculated according to $D_i = \omega_o^2/4\tau_{\mathrm{diff,i}}$ if the lateral radius, ω_o, of the detection volume is known from a calibration measurement. Furthermore, if the viscosity η of the medium is known, the Stokes-Einstein relationship,

$$D = kT/6\pi\eta R_h \quad (6)$$

allows for evaluation of the hydrodynamic radius R_h of the diffusing particles.

In addition to nonlinear least-squares fitting of the model equations to the experimental autocorrelation curves, the characteristic diffusion time τ_{diff} can be directly estimated from the half-value decay of the autocorrelation curve:

$$G_{\mathrm{Diff}}(\tau_{\mathrm{diff}}) = \frac{1}{2}\cdot G_{\mathrm{Diff}}(0) \quad (7)$$

in all cases that can be approximated by Eq. 4.

In dual-color cross-correlation (Schwille et al., 1997) the fluorescence emission signals from the two dyes are separately detected and, in addition

to the autocorrelation, the cross-correlation function is calculated (Fig. 1 and Eq. 1 with $i \neq j$).

Considering the diffusion of multiple species with two different labels, but also a distribution of different brightness values η_i of each label, the amplitude of the autocorrelation curve obtained from the green channel, for example, is determined by

$$G_g(0) = \frac{1}{N_{total,eff}} \left(\sum_k Y_k \eta_{k(g)}^2 \right) \Big/ \left(\sum_k Y_k \eta_{k(g)} \right)^2 \quad (8)$$

with Y_k being the fraction and $\eta_{k(g)}$ the brightness of species k in the green channel, as it follows from Eq. 2 for $\tau = 0$, whereas the cross-correlation amplitude is determined by

$$G_{rg}(0) = \frac{1}{N_{total,eff}} \left(\sum_k Y_k \eta_{k(r)} \eta_{k(g)} \right) \Big/ \left[\left(\sum_k Y_k \eta_{k(r)} \right) \cdot \left(\sum_k Y_k \eta_{k(g)} \right) \right] \quad (9)$$

This is only accurate for ideal setups with identically sized and completely overlapping detection volumes for the two colors and in the absence of detector cross-talk.

Formalism for cross-correlation arising from the accumulation of two kinds of single-labeled molecules in endosomal vesicles

To illustrate the significance of Eq. 9, we first consider the special case of a mixture of only three species: the first one being green with the fraction Y_g and the brightness parameters $\eta_{g(g)} = \eta_{green}$ and $\eta_{g(r)} = 0$; the second one being red with the fraction Y_r and the brightness parameters $\eta_{r(g)} = 0$ and $\eta_{r(r)} = \eta_{red}$; and the third one being both red and green with the fraction $Y_{rg} = 1 - Y_r - Y_g$ and the brightness values $\eta_{rg(g)} = \eta_{green}$ and $\eta_{rg(r)} = \eta_{red}$.

It follows from Eq. 8 and 9 that

$$\frac{G_{rg}(0)}{G_r(0) \cdot G_g(0)} = Y_{rg} \cdot N_{total,eff} = N_{rg,eff} = \langle c_{rg} \rangle \cdot V_{eff} \quad (10)$$

Thus, the cross-correlation amplitude is directly proportional to the concentration of double-labeled (red and green) species.

When single-labeled molecules accumulate in endosomal vesicles that diffuse through the focus as small single entities, the simple expression as in Eq. 10 does not hold. Rather, a distribution of different brightness values in the two channels must be taken into account. For simplicity, each endosomal vesicle is assumed to have exactly n receptor sites occupied, i.e., that each vesicle contains the same overall number of single-labeled molecules. The set of single-labeled molecules in a vesicle consists of a mixture of red and green ones. Assuming an excess of cargo molecules outside the cell and identical binding affinities of the two species to the receptor, the binding/uptake probability for a single red molecule, $p_{red} = p$, and the binding/uptake probability for a single green molecule, $p_{green} = 1 - p$, are determined by the fraction of red and green molecules outside the cells. Incomplete and uneven protein labeling are neglected. The probability of having exactly k red molecules (of n total) in a vesicle is then given by the binomial distribution:

$$P(k) = \binom{n}{k} \cdot p^k \cdot (1-p)^{n-k} \quad (11)$$

Substitution into Eq. 8 and 9, with $Y_k = P(k)$, $\eta_{k(r)} = k \cdot \eta_{red}$ and $\eta_{k(g)} = (n - k) \cdot \eta_{green}$ (assuming no quenching of the accumulated chromophores in the vesicle), yields for the cross- and the red autocorrelation amplitudes, provided an ideal optical setup:

$$G_{rg}(0) = \frac{\sum_{k=0}^{n} k(n-k) \binom{n}{k} p^k (1-p)^{n-k}}{N_{vesicles} n^2 p(1-p)} \quad (12)$$

$$G_r(0) = \frac{\sum_{k=0}^{n} k^2 \binom{n}{k} p^k (1-p)^{n-k}}{N_{vesicles} n^2 p^2} \quad (13)$$

The derivation for the green autocorrelation amplitude is analogous. Fig. 2 shows a simulation of how the cross-correlation amplitude increases depending on the number of single-labeled particles n that are incorporated into one vesicle for the simple case of $p = 0.5$, i.e., equal amounts of red and green particles outside the cell. If only one particle was taken up by each vesicle, there would be no cross-correlation. In the limit of a high number of particles per vesicle, the cross-correlation amplitude in the model approaches the autocorrelation amplitudes. (Uptake probabilities p_{red} and p_{green} do not need to be equal.)

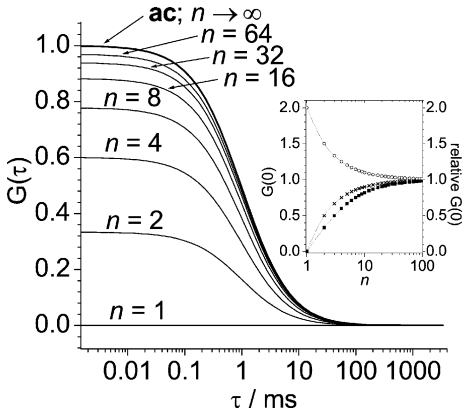

FIGURE 2 Simulation. Cross-correlation arising from the accumulation of single-labeled molecules with two different labels in vesicles. The curves were simulated for ideal setups according to Eqs. 12 and 13. The left graph shows an autocorrelation curve normalized to 1 (*ac*) and the cross-correlation curves (with amplitudes relative to *ac*) for increasing numbers of molecules per vesicle ($n = 1$ to $n \rightarrow \infty$) in the case of equal uptake probabilities for both kinds of molecules ($p = 0.5$). If only one molecule ($n = 1$) is taken up into each vesicle, cross-correlation is zero. The cross-correlation amplitude increases with the number of molecules per vesicle. In the limit of $n \rightarrow \infty$, it approaches the autocorrelation amplitudes. The inset graph shows amplitudes only: red and green autocorrelation amplitudes ($G_r(0) = G_g(0)$, ○), cross-correlation amplitudes ($G_{rg}(0)$, ×) and relative cross-correlation amplitudes ($G_{rg}(0)/G_r(0) = G_{rg}(0)/G_g(0)$, ■) all for $N_{total,eff} = 1$.

Effects of incomplete overlap of detection volumes

Diffusional cross-correlation analysis is critically dependent on the overlap of the detection volumes, because for nonperfectly overlapping detection volumes, the maximum cross-correlation amplitude relative to the autocorrelation amplitudes is reduced (Schwille, 2001b). Incomplete detection volume overlap also accounts for the fact that we observe a larger apparent diffusion time in the cross-correlation curve than in both autocorrelation curves (manuscript in preparation). With

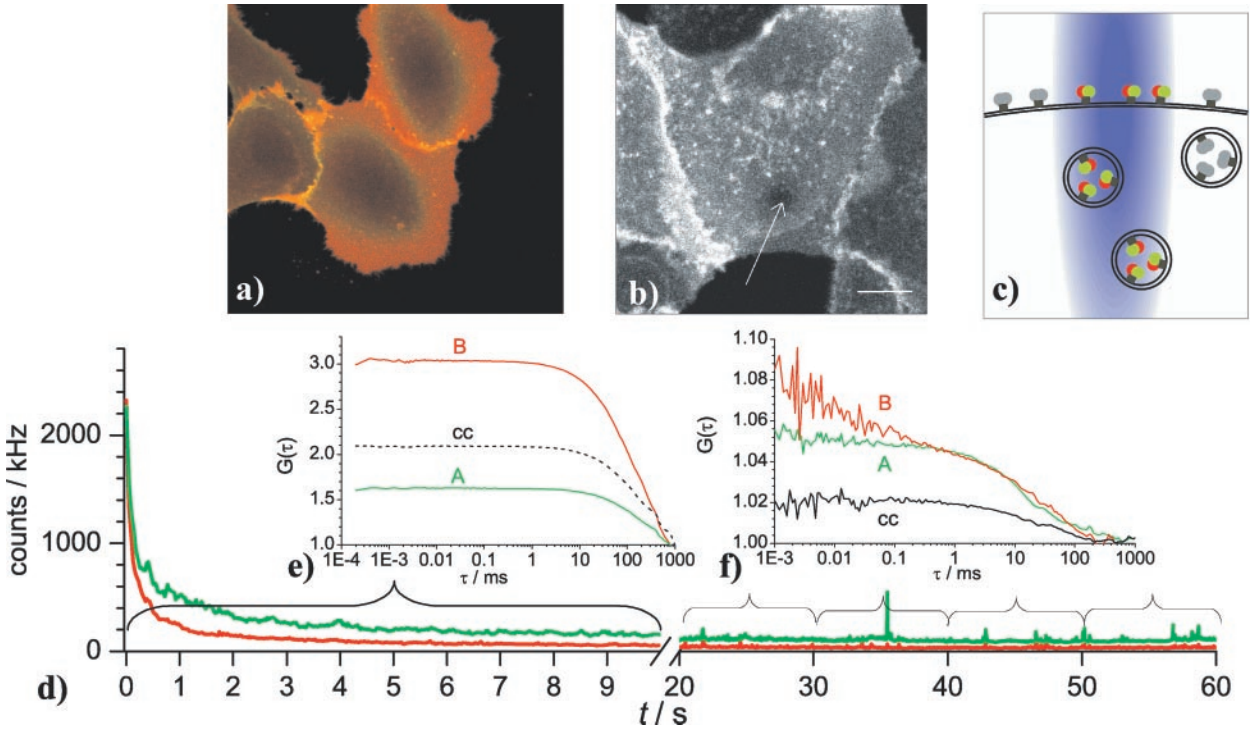

FIGURE 3 Double-labeled CTX at the plasma membrane. (*a*) LSM image of the lower membrane of Vero cells with bound double-labeled CTX. (*b*) Image taken after the attempt to measure fluorescence correlation at the position indicated by the arrow. The fluorescent CTX was bleached because of its low mobility. (*c*) Schematic representation of the FCS focus positioned on the plasma membrane: both CTX bound to the plasma membrane and CTX taken up into vesicles near the membrane are detected. (*d*) Decay in the fluorescent trace measured at the plasma membrane. The plasma membrane bound CTX bleaches away quickly because of its low mobility. (*e*) Correlation curves of the first 10 s of the dual-color FCS measurement (A: Cy2 label on the A subunit, B: Cy5 label on the B subunits, cc: artifactual cross-correlation). Auto- and cross-correlation could not be performed because of the bleaching; the cross-correlation amplitude seen here is an artifact. (*f*) Average correlation curves of the last 4 × 10 s of the FCS measurement (A: Cy2 label on the A subunit, B: Cy5 label on the B subunits, cc: cross-correlation). After most of the membrane-bound CTX was bleached, some mobile double-labeled toxin, probably already located in intracellular vesicles (Fig. 3 *c*), gave rise to cross-correlation.

the objective of maximizing the overlap of the two detection volumes, the pinhole in the red detection channel was adjusted using the 488-nm instead of the 633-nm excitation line, improving the cross-correlation amplitude by >10% on our system. Cross-correlation performance was tested using two annealed DNA oligonucleotides, labeled with rhodamin green and Cy5 in buffer solution, as described in Schwille et al. (1997). Such careful pinhole adjustment also allowed for cross-correlation analysis of 2-D membrane diffusion.

RESULTS AND DISCUSSION

Endocytosis of CTX, codiffusion, and separation of A and B subunits

Fig. 3 *a* shows a confocal laser scanning image obtained at the membrane of the Vero cell that faces the coverslip, after addition of double-labeled CTX. Toxin binds to the membrane (Fig. 3 *a*) and starts to be internalized into vesicles (Fig. 3 *b*). Attempts to perform steady-state FCS measurements on the membrane failed because of rapid bleaching, evidenced by a fast decay in the fluorescence count-rate (Fig. 3 *d*) and the presence of a dark spot seen in the subsequent LSM image (Fig. 3 *b*) after several 10-s exposures to the FCS laser focus. Such bleaching effects are usually observed if the chromophores exhibit a very low mobility and thus a long ($\gtrsim$1 s) residence time in the FCS focus. Consequently, the strong bleaching observed at moderate laser intensities (13 and 2 μW) indicates a low mobility of the membrane-bound CTX ($\lesssim 10^{-10}$ cm^2/s). During this initial phase of strong bleaching, cross-correlation analysis is precluded, as the simultaneous decay of the count-rate in both channels gives rise to an artifactual cross-correlation amplitude (Fig. 3 *e*).

The remaining fluorescence fluctuations to be seen after the initial strong bleaching period gave rise to auto- and cross-correlation curves (Fig. 3 *f*) that can most likely be ascribed to toxin that has already been taken up into vesicles, as these curves are similar to those observed intracellularly (Fig. 4). The vesicles diffuse through the laser focus on the intracellular side of the membrane (Fig. 3 *c*).

Fig. 4, *a–c*, shows confocal images recorded at a later time (15 min), when CTX has already been taken up into vesicular structures. Most of the intracellular measurements exhibited strong cross-correlation, showing that the B and A subunits of the CTX were still diffusing in

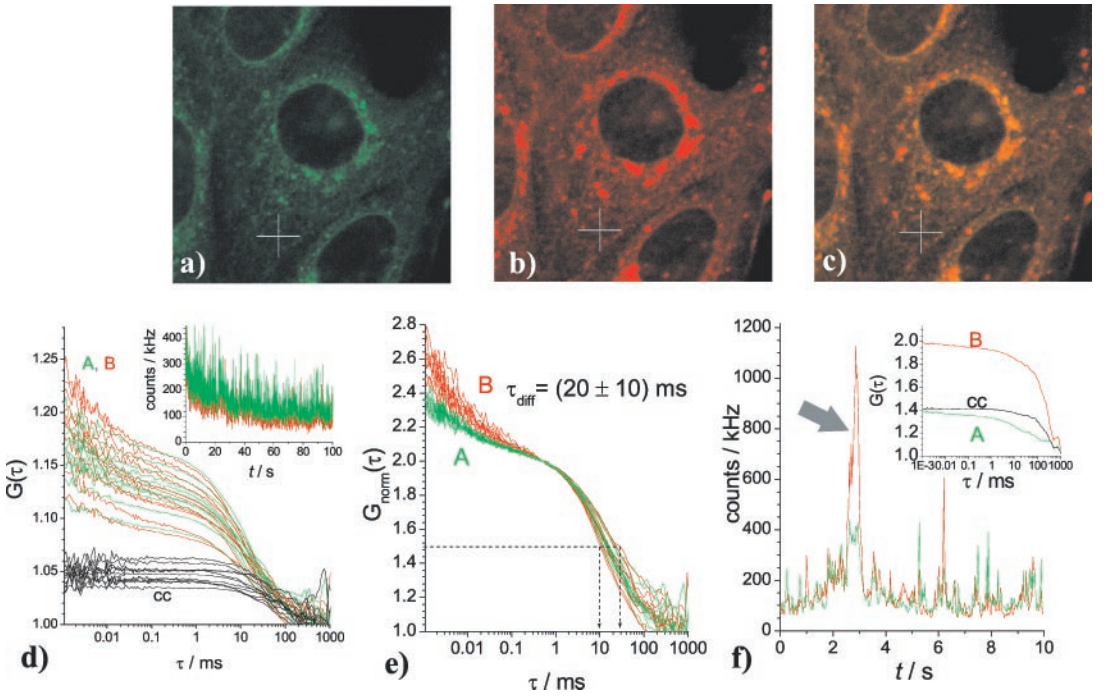

FIGURE 4 Double-labeled CTX localized in endosomes. Fig. (*a–c*) shows an LSM image taken ~15 min after the addition of double-labeled CTX ((*a*): Cy2 channel, (*b*): Cy5 channel, (*c*): overlay). The cross-hair indicates the position where the corresponding fluorescence correlation measurement is taken. Graphs (*d*) and (*e*) represent this intracellular fluorescence correlation measurement: green lines correspond to the Cy2 signal from the A subunit, red lines to the Cy5 signal from the B subunits, black lines are cross-correlation curves. (*d*) Auto- and cross-correlation curves of 10 successive measurements of 10-s duration each, at the position indicated in the images above. As is evident from the similarity of the curves, the initial decrease in the count-rate traces (*inset*) does not cause artifacts. (*e*) Autocorrelation curves after amplitude normalization. The diffusion time of the vesicles is (20 ± 10) ms. (*f*) In some intracellular measurements, correlation curves (*inset*) are dominated by singular, bright events in the count-rate trace (*arrow*), presumably brought about by large, brightly stained structures.

a coordinated fashion (Fig. 4 *d*). They may be directly bound to one another, or they may simply be confined to the *same* vesicles. Residual bleaching effects as indicated by the count-rate (Fig. 4 *d*, inset) at the beginning of a measurement series do not corrupt the cross-correlation signal, because all auto- and cross-correlation curves in 10 × 10-s correlation intervals exhibit very similar functional forms (Fig. 4 *d*), although their absolute amplitudes differ. This indicates that the local concentrations were fluctuating with time in the measurement spot. For an impression of particle mobility and the representation of double-labeled species, all measured curves were averaged (Fig. 6 *b*). In Fig. 4 *e*, autocorrelation curves were normalized at the transition between the blinking and the diffusion decays at ~0.5 ms. The average diffusion time derived by fitting the curves according to Eqs. 3 and 5 was (20 ± 10) ms, corresponding to an average diffusion coefficient of $D = 6 \cdot 10^{-9}$ cm^2/s based on the calibration of the detection volumes. Using the Stokes-Einstein relationship and assuming a relative cytosolic viscosity of $\eta \approx 5$, this relates to a hydrodynamic diameter of $2R_h \approx 150$ nm, which is a reasonable value for endosomes (Mukherjee et al., 1997). However, in a few of the 10-s measurement intervals, pronounced spikes in the count-rate trace (Fig. 4 *f*) lead to correlation curves that were dominated by these singular events (Fig. 4 *f*, inset). These spikes may be attributed to very large mobile structures containing much more labeled CTX molecules, such as multivesicular bodies or moving tubular structures.

Further along the endocytic pathway, CTX accumulates in the Golgi apparatus (Fig. 5 *a*). In a similar fashion as at the membrane, a relatively strong initial bleaching can be observed in the count-rate trace (Fig. 5 *b*), indicating that the CTX in the Golgi was mostly immobilized because of confinement or binding, presumably by membrane localization. However, after the prevalent immobile fraction was bleached away, the remaining fraction showed a significantly reduced relative cross-correlation amplitude compared with cytoplasmic measurements (Fig. 5 *c*, compared with Fig. 4 *d* or Fig. 6 *b*). In agreement with this, the diffusion characteristics of the two labels differed significantly (Fig. 5 *c*). Both the loss of cross-correlation and the difference in diffusion times strongly support the hypothesis that the A subunit becomes separated from the B subunit in the Golgi (Bastiaens et al., 1996).

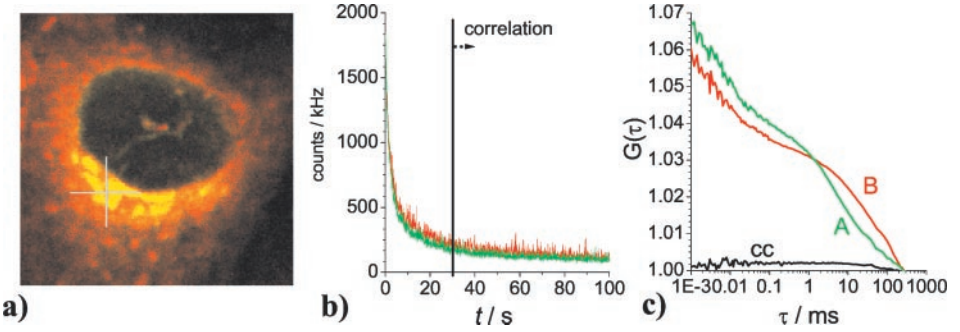

FIGURE 5 Double-labeled CTX in the Golgi. (*a*) LSM image showing the brightly stained Golgi apparatus and the position of the following FCS measurement (*cross-hair*). (*b*) Count-rate traces of the fluorescence correlation measurement with the focus positioned in the Golgi apparatus area. (*c*) Correlation analysis performed after the strong initial bleaching reveals that the mobile fraction exhibits a significantly reduced cross-correlation amplitude and differing diffusion characteristics of A and B subunits.

Cargoes following the same pathway cause cross-correlation

The diffusion times observed for cytoplasmic diffusion (τ_{diff} = 10–30 ms) already indicate that the motion of vesicles rather than of single protein complexes was being observed. To confirm this, we investigated the endocytosis of a mixture of single-labeled holotoxins. As opposed to the double-labeled toxin molecules, which already give rise to cross-correlation in buffer solution (Fig. 6 *a*), no cross-correlation was observed for a mixture of single-labeled toxin complexes under the same conditions in vitro (Fig. 6 *c*). Nevertheless, when the mixture of single-labeled toxins was endocytosed by the cell, they exhibited strong cytoplasmic cross-correlation (Fig. 6 *d*), similar to the endocytosis of double-labeled toxin complexes (Fig. 6 *b*). Therefore, the previous independently moving toxin molecules labeled with one or the other dye became confined to the same small vesicle and thereby showed cross-correlated motion. This implies that the utilization of the same endocytic pathway by different endocytic cargoes may be recognized by simply providing the labeled cargoes to the cells and subsequently performing cross-correlation measurements on the live cells. Fluorescence cross-correlation analysis therefore provides the fascinating perspective to quickly and reliably evaluate the utilization of endocytic pathways by various cargoes. Further experimental evidence of this concept with different types of cargoes is currently being investigated (manuscript in preparation).

Significance of cross-correlation amplitudes

Chemical amino-reactive labeling of a protein such as CTX produces a heterogeneous sample with variable numbers of

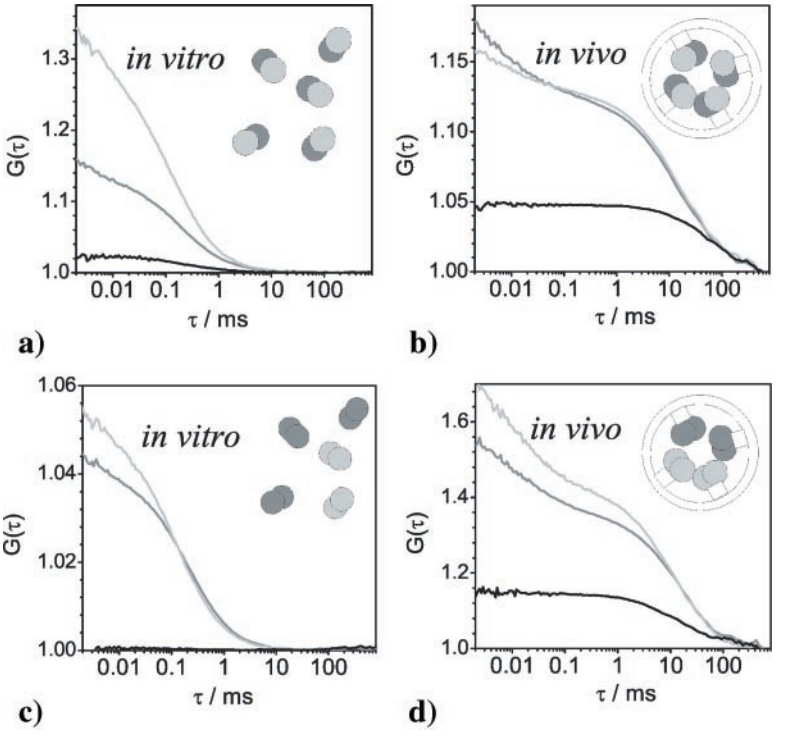

FIGURE 6 Comparison of the cross-correlation from single- and double-labeled toxin, in vitro and in vivo. The light gray and dark gray lines denote the autocorrelation curves of the Cy2 signal and the Cy5 signal, respectively. The black line represents the cross-correlation of the two channels. (*a*) Double-labeled CTX in buffer solution shows cross-correlation. (*b*) Intracellular measurement of double-labeled CTX that has been endocytosed into vesicles. (*c*) A mixture of Cy2 and Cy5 single-labeled holotoxin molecules in solution shows no cross-correlation. (*d*) Intracellular measurement of a mixture of single-labeled holotoxins. The high cross-correlation amplitude suggests that the joint usage of a certain type of vesicles by different cargoes may be recognized by using fluorescence *cross*-correlation analysis.

chromophores linked to each subunit. This causes nonuniform brightness distributions within the protein sample and impedes a straightforward interpretation of both auto- and cross-correlation amplitudes. For example, it is evident that in cross-correlation analysis, incomplete labeling leading to molecules that carry only Cy2 labels and others that carry only Cy5 labels causes a reduced cross-correlation amplitude. In particular, the stringent labeling conditions used in our experiments to minimize undesired "cross-labeling", i.e., to ensure that only A subunits are labeled with Cy2 and only B subunits are labeled with Cy5 resulted in the creation of many single-labeled molecules lowering the cross-correlation amplitudes as seen in Fig. 6 *a*.

However, when *n* molecules are taken up by a single diffusing vesicle (Fig. 6 *b*), it becomes less relevant whether they are completely double-labeled. The more molecules (*n*) are enclosed in each vesicle, the greater the probability to detect double-labeled entities. This increases the amplitude of the cross-correlation generated by accumulation of two different dyes in the same vesicle, even if the molecules are just single-labeled (Fig. 6 *d*). These intracellular measurements obtained from cells that were endocytosing a mixture of Cy2- and Cy5-labeled holotoxins yielded cross-correlation amplitudes mainly at ~0.4, but up to 0.7, relative to the lower autocorrelation. These experimental cross-correlation amplitudes can be rationalized based on our model described in Materials and Methods. Fig. 2 depicts the cross-correlation curves expected from vesicles containing *n* single-labeled molecules in ideal setups, computed from the model Eqs. 12 and 13 for the simplest case of $p = 0.5$ (same overall number of red and green molecules). The inset shows the relative cross-correlation *amplitudes* versus the number of toxin molecules in the vesicle. When comparing the measured cross-correlation amplitudes with the model with the aim of deducing the number of molecules per vesicle, nonidealities should be taken into account, particularly incomplete detection volume overlap, which reduces the cross-correlation amplitude. Calibration experiments introduced by Schwille et al. (1997) have shown that a maximum cross-correlation amplitude of 0.8 can be obtained with our setup. Therefore, the corrected experimental cross-correlation amplitudes ranged between 0.5 and 0.88 and corresponded to at least 3 to 15 particles per vesicle according to Eqs. 12 and 13 and Fig. 2. This is a lower limit, because any non–cross-correlated background, e.g., arising from cellular autofluorescence or degraded labeled proteins, also reduces the cross-correlation amplitude. Fortunately, the experimental cross-correlation amplitudes were high compared with in vitro measurements of double-labeled CTX, because the good signal in our curves allows for a reliable detection of concomitant movement.

It should be mentioned that the fast (<100 μs) dynamics observed in the autocorrelation curves of the cyanine dyes provide a valuable tool for distinguishing real cross-correlation from artifactual cross-correlation arising from detector cross-talk. The relative fractions of these fast dynamics were relatively large, even at low excitation intensities, probably because of an isomerization reaction in the fluorophores (Widengren and Schwille, 2000). These conversions to the dark states occur independently in both fluorophores on the same particle and are therefore not cross-correlated. Only fast fluctuations from the same chromophore appearing in both channels because of detector cross-talk would cross-correlate and would consequently appear in the cross-correlation curve (Schwille et al., 1997). Because of the absence of cross-correlated fast dynamics in our experiments, the cross-correlation must be attributed to the concomitant movement of the two labeled molecules and not to cross-talk. In addition, this confirms the discrimination in time ranges between dye dynamics and particle diffusion dynamics.

Lateral mobility of CTX bound to GM1 in membranes

For GM1-bound membrane-localized CTX, we encountered bleaching because of very low mobility and were unable to perform FCS measurements (Fig. 3). On the contrary, diffusion of lipids or membrane-associated proteins is generally well accessible by FCS. For example, using the same setup, we analyzed the diffusion of the lipid analogue $diIC_{18}$ (1, 1′-dioctadecyl-3, 3, 3′, 3′-tetramethylindocarbocyanine) in the plasma membrane of rat basophilic leukemia cells (Schwille et al., 1999b), which was on the order of 10^{-9} cm^2/s (data not shown). The same lipid analogue $diIC_{18}$ exhibits ~10 times faster diffusion ($D = (6 \pm 1) \times 10^{-8}$ cm^2/s, data not shown) in DLPC-GUVs than in the cellular plasma membrane. Interestingly, CTX bound to GM1-containing DLPC-GUVs was approximately equally mobile ($D = (5 \pm 1) \times 10^{-8}$ cm^2/s, Fig. 7 *b*). The strong immobilization of GM1, but not of $diIC_{18}$ in the cell plasma membrane compared with the artificial DLPC membrane may be attributed to the alleged raft-association of GM1 and merits further investigations.

Performing cross-correlation analysis on membranes

In principle, ligand receptor binding can be measured by fluorescence *auto*correlation on membranes, because the free ligand, in our experiments CTX (Fig. 7 *a*, $D = (5 \pm 1) \times 10^{-7}$ cm^2/s) and the receptor-bound ligand (Fig. 7 *b*, $D = (5 \pm 1) \times 10^{-8}$ cm^2/s) exhibit different diffusion times. When more ligand is added (Fig. 7, *c* and *d*), the autocorrelation curve necessitates a two-component fit to include both the membrane-bound and the free ligand (Fig. 7 *d*, fractions were evaluated from the two-component fit). A number of these autocorrelation studies have previously been performed (Rigler et al., 1999; Pramanik and Rigler,

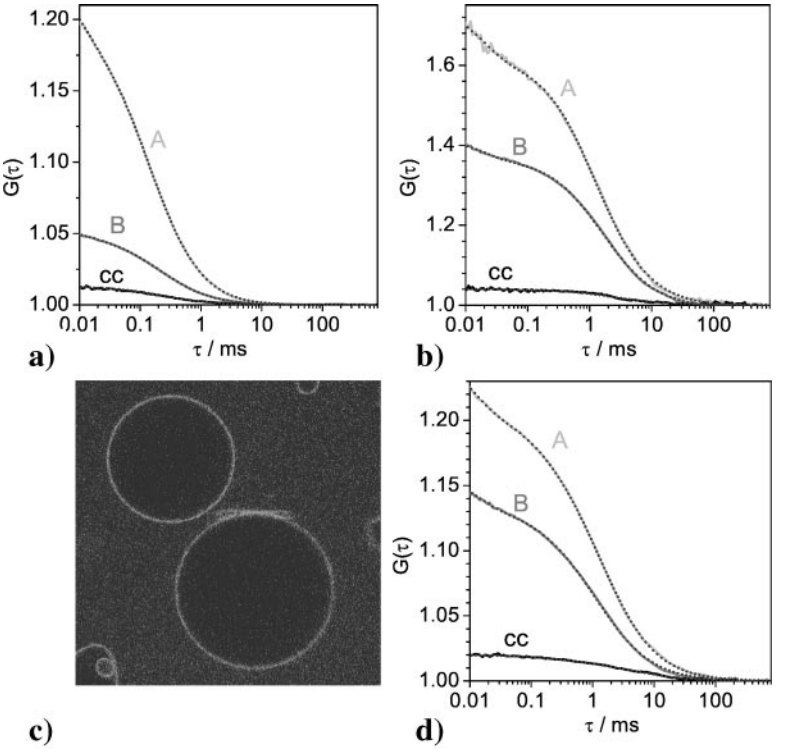

FIGURE 7 Measuring cross-correlation on membranes. Light gray lines correspond to Cy2 labels on A subunits, dark gray lines to Cy5 labels on the B subunits, and black lines to cross-correlation curves. Dotted lines represent nonlinear least squares fits. (*a*) Dual-color cross-correlation measurement of double-labeled CTX in buffer solution. The fit to a one-component diffusion model yields a diffusion coefficient of $D = 5 \cdot 10^{-7}$ cm^2/s. (*b*) Dual-color cross-correlation measurement of double-labeled CTX bound to GM1 in a DLPC-GUV membrane. The relative concentration of free CTX is very low, which allows fitting to a one-component diffusion model, resulting in $D = 5 \cdot 10^{-8}$ cm^2/s. (*c*, *d*) With more free ligand outside the GUVs, the fluorescence correlation curves measured on the membrane must be fitted to a two-component diffusion model, yielding an 80% fraction of bound toxin and a 20% fraction of free toxin in this particular measurement.

2001) on cell membranes, where the fractions of free ligand and membrane-bound ligand were calculated by evaluating distributions of diffusion times with a special algorithm (CONTIN). In these experiments, membrane diffusion times presumably ranged from $D = 2 \times 10^{-7}$ cm^2/s to $D = 2 \times 10^{-10}$ cm^2/s (τ_{diff} = 1–700 ms, setup with $\omega_o = 0.25$ μm), illustrating that there are ligand-receptor systems of pharmacological interest which are amenable to FCS. Nevertheless, the discrimination of fractions from autocorrelation curves is rather difficult, and the results might be dependent on the positioning of the focus on the membrane. We now show that with careful adjustment of the setup, cross-correlation analysis can be applied to membranes. Double-labeled CTX bound to GM1-containing DLPC-GUVs exhibits cross-correlation (Fig. 7 *d*). This opens the door to improving ligand-membrane receptor binding analysis by labeling the receptor and the ligand with appropriate, distinguishable dyes and performing *cross*-correlation analysis on the membrane.

CONCLUSIONS

We have applied dual-color fluorescence cross-correlation to follow endocytosis of the CTX AB_5 complex and the separation of the A and B subunits in vivo. Our findings confirm the hypothesis previously found using FRET in fixed cells, that a complete separation of subunits does not occur before the toxin cargo has reached the Golgi apparatus. Second, we found that CTX bound to its supposedly raft-associated plasma membrane receptor, GM1, is immobilized on the FCS time scale, but that cross-correlation analysis is in principle applicable to the 2-D system of lipid membranes. Finally, we have shown that simultaneous endocytosis of two differently single-labeled toxins gives rise to significant cross-correlation, suggesting a new, dynamic approach for studying coincidence in endocytic pathways.

FRET could not be used to study the colocalization of cargoes in the same endocytic vesicles because the molecules in the vesicle are not necessarily in the close proximity required for FRET. The advantage of fluorescence fluctuation cross-correlation analysis compared with (confocal) fluorescence imaging is that it involves the dimension of time, i.e., it selectively probes the concomitant *movement* of the differently colored particles through the focus. In contrast, traditional microscopic colocalization assessment (Ghosh et al., 1994) and quantitative analysis of confocal laser scanning microscope images by spatial cross-correlation (Petersen, 2001) probe a stationary coincidence between two images on the scale of optical resolution at the moment of image acquisition. Exploiting the dimension of time eliminates the difficulty of accounting for random colocalization of fluorescent signals in images. Thus, dual-color cross-correlation analysis can be considered a dynamic analogue to colocalization, with the important advantage of considerably reduced false-positive signals attributable to the extremely low probability of coordinated fluctuations of two fully independent measurement parameters. Furthermore, fluorescence cross-correlation provides

a less biased analysis. For example, it avoids biases from individual settings of LSM parameters, such as the photomultiplier voltage that influences pixel saturation, image presentation parameters, such as brightness and contrast, and image analysis parameters such as thresholds. This facilitates the analysis of endosomal colocalization and renders it less susceptible to inadvertent biases. Because FCS can only be used if the particles are sufficiently mobile, this technique is best suited for analyzing steps in endocytic pathways where the cargo is located in small moving vesicles. As these vesicles are below the resolution of colocalization studies using LSM and the distances between the cargo molecules in the vesicles are generally out of the range suitable for FRET techniques, fluorescence cross-correlation analysis may prove to be an extremely useful complementary technique. We are still far from a complete understanding of the complex network of endocytosis, but as a number of (endosomal) markers have been identified, one can now attempt to analyze the cross-correlation of different markers with different cargoes during the time course of internalization.

We thank Dag Scherfeld for preparation of the GUVs, other members of the Experimental Biophysics group for helpful discussions, and Sally Kim for proofreading the manuscript. The study was carried out in collaboration with Carl Zeiss (Jena, Germany). Financial support was provided by the Volkswagen Foundation (grant no. I/76 676), the German Ministry of Education and Research (grants no. 0311845 and 16SV1257), and Evotec OAI (Hamburg, Germany).

REFERENCES

Akashi, K., H. Miyata, H. Itoh, and K. Kinosita, Jr. 1996. Preparation of giant liposomes in physiological conditions and their characterization under an optical microscope. *Biophys. J.* 71:3242–3250.

Bastiaens, P. I., I. V. Majoul, P. J. Verveer, H. D. Söling, and T. M. Jovin. 1996. Imaging the intracellular trafficking and state of the AB5 quaternary structure of cholera toxin. *EMBO J.* 15:4246–4253.

Brock, R., M. Hink, and T. M. Jovin. 1998. Fluorescence correlation microscopy of cells in the presence of autofluorescence. *Biophys. J.* 75:2547–2557.

Eigen, M., and R. Rigler. 1994. Sorting single molecules: applications to diagnostics and evolutionary biotechnology. *Proc. Natl. Acad. Sci. U.S.A.* 91:5740–5747.

Elson, E. L., and D. Magde. 1974. Fluorescence correlation spectroscopy. I. Conceptual basis and theory. *Biopolymers.* 13:1–27.

Elson, E. L., and R. Rigler, editors. 2001. Fluorescence Correlation Spectroscopy: Theory and Applications. Springer, Berlin.

Fontana, M.R., R. Manetti, V. Giannelli, C. Magagnoli, A. Marchini, R. Olivieri, M. Domenighini, R. Rappuoli, and M. Pizza. 1995. Construction of nontoxic derivatives of cholera toxin and characterization of the immunological response against the A subunit. *Infect. Immun.* 63: 2356–2360.

Ghosh, R. N., D. L. Gelman, and F. R. Maxfield. 1994. Quantification of low density lipoprotein and transferrin endocytic sorting in HEp2 cells using confocal microscopy. *J. Cell Sci.* 107:2177–2189.

Heinze, K. G., A. Koltermann, and P. Schwille. 2000. Simultaneous two-photon excitation of distinct labels for dual-color fluorescence cross-correlation analysis. *Proc. Natl. Acad. Sci. U.S.A.* 97: 10377–10382.

Kettling, U., A. Koltermann, P. Schwille, and M. Eigen. 1998. Real time enzyme kinetics of restriction endonuclease *Eco*RI monitored by dual-color fluorescence cross-correlation spectroscopy. *Proc. Natl. Acad. Sci. U.S.A.* 95:14116–11420.

Lencer, W. I., T. R. Hirst, and R. K. Holmes. 1999. Membrane traffic and the cellular uptake of cholera toxin. *Biochim. Biophys. Acta.* 1450: 177–190.

Magde, D., E. L. Elson, and W. W. Webb. 1972. Thermodynamic fluctuations in a reacting system: measurement by fluorescence correlation spectroscopy. *Phys. Rev. Lett.* 29:705–708.

Majoul, I. V., P. I. Bastiaens, and H. D. Söling. 1996. Transport of an external Lys-Asp-Glu-Leu (KDEL) protein from the plasma membrane to the endoplasmic reticulum: studies with cholera toxin in Vero cells. *J. Cell Biol.* 133:777–789.

Mukherjee, S., R. N. Ghosh, and F. R. Maxfield. 1997. Endocytosis. *Physiol. Rev.* 77:760–803.

Petersen, N. O. 2001. FCS and spatial correlations on biological surfaces. *In* Fluorescence Correlation Spectroscopy: Theory and Applications. E.L. Elson and R. Rigler, editors. Springer, Berlin. 162–184.

Pramanik, A., and R. Rigler. 2001. FCS-analysis of ligand-receptor interactions in living cells. *In*: Fluorescence Correlation Spectroscopy: Theory and Applications. E.L. Elson and R. Rigler, editors. Springer, Berlin. 101–131.

Rigler, R., Ü. Mets, J. Widengren, and P. Kask. 1993. Fluorescence correlation spectroscopy with high count rates and low background: analysis of translational diffusion. *Eur. Biophys. J.* 22:169–175.

Rigler, R., A. Pramanik, P. Jonasson, G. Kratz, O. T. Jansson, P. A. Nygren, S. Stahl, K. Ekberg, B. L. Johansson, S. Uhlen, M. Uhlen, H. Jornvall, and J. Wahren. 1999. Specific binding of proinsulin C-peptide to human cell membranes. *Proc. Natl. Acad. Sci. U.S.A.* 96: 13318–13323.

Schiavo, G., and F. G. van der Goot. 2001. The bacterial toxin toolkit. *Nat. Rev. Mol. Cell Biol.* 2:530–537.

Schwille, P. 2001a. Fluorescence correlation spectroscopy and its potential for intracellular applications. *Cell. Biochem. Biophys.* 34:383–408.

Schwille, P. 2001b. Cross-correlation analysis in FCS. *In* Fluorescence Correlation Spectroscopy: Theory and Applications. E.L. Elson and R. Rigler, editors. Springer, Berlin. 360–378.

Schwille, P., U. Haupts, S. Maiti, and W. W. Webb. 1999a. Molecular dynamics in living cells observed by fluorescence correlation spectroscopy with one- and two-photon excitation. *Biophys. J.* 77:2251–2265.

Schwille, P., J. Korlach, and W. W. Webb. 1999b. Fluorescence correlation spectroscopy with single molecule sensitivity on cell and model membranes. *Cytometry.* 36:176–182.

Schwille, P., S. Kummer, A. A. Heikal, W. E. Moerner, and W. W. Webb. 2000. Fluorescence correlation spectroscopy reveals fast optical excitation-driven intramolecular dynamics of yellow fluorescent proteins. *Proc. Natl. Acad. Sci. U.S.A.* 97:151–156.

Schwille, P., F.-J. Meyer-Almes, and R. Rigler. 1997. Dual-color fluorescence cross-correlation spectroscopy for multicomponent diffusional analysis in solution. *Biophys. J.* 72:1878–1886.

Thompson, N. L. 1991. Fluorescence correlation spectroscopy. *In* Topics in Fluorescence Spectroscopy, Vol. 1: Techniques. J. R. Lakowicz, editor. Plenum Press, New York.

Wachsmuth, M., W. Waldeck, and J. Langowski. 2000. Anomalous diffusion of fluorescent probes inside living cell nuclei investigated by spatially-resolved fluorescence correlation spectroscopy. *J. Mol. Biol.* 298:677–689.

Widengren, J., Ü. Mets, and R. Rigler. 1995. Fluorescence correlation spectroscopy of triplet states in solution: a theoretical and experimental study. *J. Chem. Phys.* 99:13368–13379.

Widengren, J., and R. Rigler. 1998. Fluorescence correlation spectroscopy as a tool to investigate chemical reactions in solutions and on cell surfaces. *Cell. Mol. Biol.* 44:857–879.

Widengren, J., and P. Schwille. 2000. Characterization of photoinduced isomerization and back-isomerization of the cyanine dye cy5 by fluorescence correlation spectroscopy. *J. Chem. Phys.* 104:6416–6428.